SCIENCE CHINA
Information Sciences

• RESEARCH PAPER •

January 2021, Vol. 64 112210:1–112210:12
https://doi.org/10.1007/s11432-019-2743-8

Line-of-sight based three-dimensional path following control for an underactuated robotic dolphin

Jincun LIU[1], Zhenna LIU[2] & Junzhi YU[1,3*]

[1]*State Key Laboratory for Turbulence and Complex System, Department of Mechanics and Engineering Science, BIC-ESAT, College of Engineering, Peking University, Beijing* 100871*, China;*
[2]*Department of Electrical and Automation, Shandong Labor Vocational and Technical College, Jinan* 250022*, China;*
[3]*State Key Laboratory of Management and Control for Complex Systems, Institute of Automation, Chinese Academy of Sciences, Beijing* 100190*, China*

Received 11 September 2019/Revised 7 November 2019/Accepted 4 December 2019/Published online 22 December 2020

Abstract This paper investigates the three-dimensional (3-D) path following control problem for an underactuated robotic dolphin. With a comprehensive consideration of the mechanical constraint and swimming principle of the robotic dolphin, a decoupling motion strategy is proposed to produce yaw and pitch maneuvers simultaneously. Then, kinematics and dynamics models for 3-D dolphin-like swimming are established, followed by simulations of the path following control. Furthermore, a novel lookahead based 3-D line-of-sight (LOS) guidance law is developed and implemented to obtain desired attitude angles with its simplicity, intuitiveness, and small computational footprint. Finally, simulation results illustrate the feasibility and effectiveness of the proposed path following control methods.

Keywords robotic dolphin, path following, 3-D, LOS guidance law, decoupling motion

Citation Liu J C, Liu Z N, Yu J Z. Line-of-sight based three-dimensional path following control for an underactuated robotic dolphin. Sci China Inf Sci, 2021, 64(1): 112210, https://doi.org/10.1007/s11432-019-2743-8

1 Introduction

Autonomous underwater vehicles (AUVs) are critical to the long-term future of marine development and protection. However, the drawbacks of traditional rotary-propeller based underwater vehicles are obvious, such as low driving efficiency, large turning radius, and much disturbance to the aquatic species. In nature, aquatic animals have been endowed with novel morphological features and incredible locomotion characteristics that enable them to cope up with different living conditions. Inspired by nature, engineers and researchers put their hands to create innovative underwater vehicles that interact with the aquatic environment friendly. In 1994, the first robotic fish was developed by MIT, which preluded bioinspired underwater robots.

As a typical marine mammal, dolphins are relatively well endowed with many novel mechanisms and astounding swimming abilities based on the vertical oscillation of the fluke and vertebral columns, such as high swimming speed, reduced detection, and enhanced maneuverability [1]. The potential applications of biomimetic dolphin-like swimming robots would apply to marine exploration, mariculture, and military affairs, which involved three-dimensional (3-D) topographic mapping, offshore aquaculture, environmental monitoring, archaeology, exploration, etc. [2]. The 3-D path following control of the robotic dolphins will be an indispensable tool to achieve the above tasks. Recently, to realize 3-D maneuver, various robotic dolphins with innovative mechanical structures have been implemented. For example, Nakashima et al. [3] presented a robotic dolphin to achieve 3-D maneuverability by offsetting the center of oscillation of the caudal fin and dorsal fin. Wu et al. [4, 5] designed a gliding robotic dolphin and achieved 3-D attitude control by adjusting the controllable fluke and flippers during the gliding process. Wang et al. [6] utilized the movable mass and dolphin-like swimming part for their gliding robotic dolphin to change the pitch and yaw angles, respectively. Yu et al. [7] built an acrobatic robotic dolphin to implement frontflip,

* Corresponding author (email: junzhi.yu@ia.ac.cn)

backflip, as well as yaw motions, which were benefited from the multiple pitch joints and yaw joint in the body. Shen et al. [8] developed a robotic dolphin with two turning units and multi-link oscillatory joints. The yaw maneuver and pitch motion were realized by controlling the turning joints and the flipper's deflection, respectively. In order to achieve 3-D motion, Wang et al. [9] proposed a robotic dolphin, whose tail was divided into three swing joints and a twist joint. However, the 3-D motion of above robotic dolphins is decoupled into the horizontal plane and vertical plane with the sacrifice of intricate mechatronic design (such as added turning joints or buoyancy-driven system). To make up for these defects, we had addressed the path following problems for a straightforward robotic dolphin in the vertical plane [10] and horizontal plane [11], respectively. Therefore, how to design the 3-D decoupling motion is worthy of more intensive investigation.

The path following problem can be regarded as the classical line-of-sight (LOS) guidance problem by steering a virtual target converges to and follows the desired waypoints, without strict temporal requirements [12, 13]. Breivik and Fossen [14] proposed the novel LOS guidance law for marine surface vessels, and then a variety of variants had been developed, such as adaptive LOS [15, 16] strategies and integral LOS [17, 18] methods, by adding adaptive and integral terms to alleviate the effects of uncertainties. However, few studies involved 3-D LOS guidance law. Lekkas [19] designed an LOS guidance law for 3-D motion, and the coupled movement was decomposed into depth controller and horizontal LOS controller. The utilized LOS guidance method was, at the bottom, horizontal guidance law. Zuo et al. [20] built a guidance based 3-D path following method that consisted of a guidance loop, an attitude stabilization loop, and a velocity tracking loop. The guidance law was utilized from [21], which was obtained through complicated derivation. Wang et al. [22] developed a fuzzy iterative sliding mode control scheme for special AUVs on the 3-D path following problem, where the 3-D LOS guidance law was utilized to offer attitude angles. However, the time-varying guidance variable was considered as a positive constant. Therefore, it is worth exploring the simple but effective 3-D guidance law.

The primary purpose of this paper is to provide a 3-D path following solution for an underactuated robotic dolphin. A brief overview of the mechatronic design and decoupling motion for the robotic dolphin is first developed to obtain a clear understanding of the 3-D maneuver. As an extension of our studies [10, 11], a lookahead based 3-D LOS guidance law is proposed. Simulations of both decoupling motion and 3-D path following are finally carried out to verify the feasibility of the proposed strategies.

The remainder of this paper is structured as follows. The mechanical design and 3-D decoupling motion of the underactuated robotic dolphin are overviewed in Section 2. The kinematic and dynamic models of 3-D swimming are detailed in Section 3, followed by the LOS guidance law in Section 4. The numerical simulations and analyses are provided in Section 5. Finally, concluding remarks and outline of future investigations are offered in Section 6.

2 Overview of the robotic dolphin

2.1 Mechatronic design

The developed robotic dolphin consists of a waist joint, a fluke, and a pair of independent mechanical flippers, whose mechanical structure is elaborated in Figure 1. For the sake of reducing hydraulic resistance, a well-streamlined shape that is loosely modeled after the killer whale is designed to offer an expected lift-to-drag ratio. To implement the dolphin-like swimming, two pitch joints are exploited to realize dorsoventral oscillations. Meanwhile, the mechanical flippers are utilized for better attitude adjustment. Furthermore, the movement of the robotic dolphin is controlled by a Raspberry Pi that is embedded in the head. Diversified onboard sensors are equipped for autonomous 3-D path following solution, such as inertial measurement unit (IMU) and pressure sensor.

2.2 3-D decoupling motion

The robotic dolphin has been developed for excellent agility on depth control [10] and planar path following control [11], while the flippers make the crucial contribution to the success of both motions. The yaw maneuver is coupling with the pitch maneuver of the robot. Therefore, the research of 3-D decoupling motion is urgent.

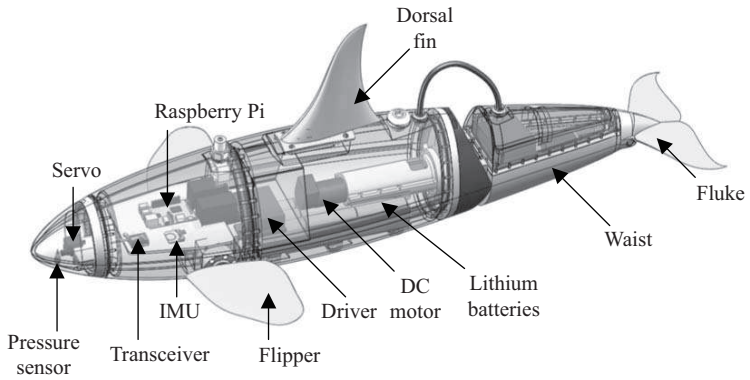

Figure 1 Illustration of the mechanical structure of the robotic dolphin.

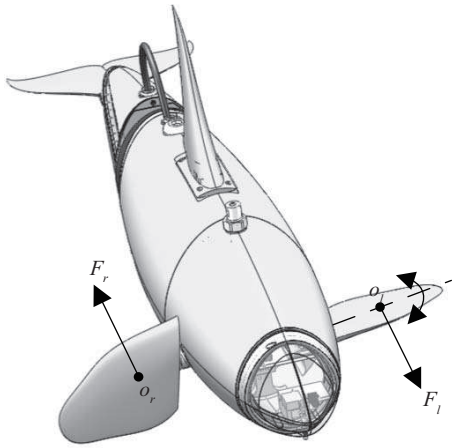

Figure 2 The yaw maneuver of the robotic dolphin.

2.2.1 *Yaw maneuver*

The asymmetric flapping of the bilateral flippers will generate different hydrodynamic forces, which produces effective yaw maneuver. Based on [23], the turning pattern named as turning with braking (unilateral flipper flapping and the other maintaining vertical) is utilized for its excellent astringency, which is plotted in Figure 2. A Hopf oscillator based on central pattern generator (CPG) model is adopted to realize smooth motion.

$$\begin{aligned} \dot{x_{\text{flip}}} &= -\omega_{\text{flip}} y_{\text{flip}} + x_{\text{flip}}(m_{\text{flip}}^2 - x_{\text{flip}}^2 - y_{\text{flip}}^2) + h_1 x_{\text{flip}-1}, \\ \dot{y_{\text{flip}}} &= \omega_{\text{flip}} x_{\text{flip}} + y_{\text{flip}}(m_{\text{flip}}^2 - x_{\text{flip}}^2 - y_{\text{flip}}^2) + h_2 y_{\text{flip}+1}, \end{aligned} \tag{1}$$

where m_{flip} and ω_{flip} represent the intrinsic amplitude and oscillation frequency of the flipper. x_{flip} and y_{flip} denote the state variables. h_1 and h_2 stand for coupling weights which can adjust the convergence speed.

2.2.2 *Pitch maneuver*

Inspired by the frontflip and backflip of the robotic dolphin in the vertical plane [7], the flexible posterior body and flukes moving in the form of body wave are forcibly deflexed or upturned to ensure an asymmetric motion (e.g., adding some biases to the waist and fluke). The diving and ascending motions are fabricated in Figure 3, and the corresponding dorsoventral oscillations equation can be simplified as

$$\begin{aligned} x_{\text{waist}} &= \varphi_{\text{waist\_offset}} + m_{\text{waist}} \sin(2\pi f t), \\ x_{\text{fluke}} &= \varphi_{\text{fluke\_offset}} + m_{\text{fluke}} \sin(2\pi f t + \zeta), \end{aligned} \tag{2}$$

where x_{waist} and x_{fluke} denote the state variables of the waist and fluke, $\varphi_{\text{waist\_offset}}$ and $\varphi_{\text{fluke\_offset}}$ mean the bias angles of the waist and fluke, m and f stand for intrinsic amplitude and oscillation frequency,

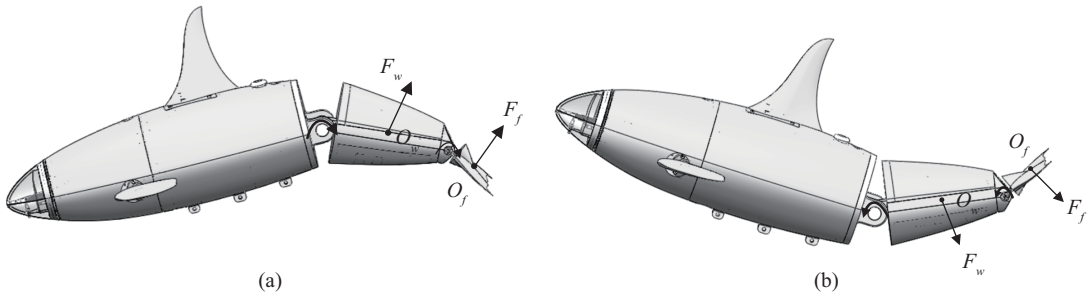

Figure 3 The illustration of pitch maneuver. (a) The diving motion in which the waist joint and fluke are forcibly deflexed; (b) the ascending motion in which the waist joint and fluke are all upturned.

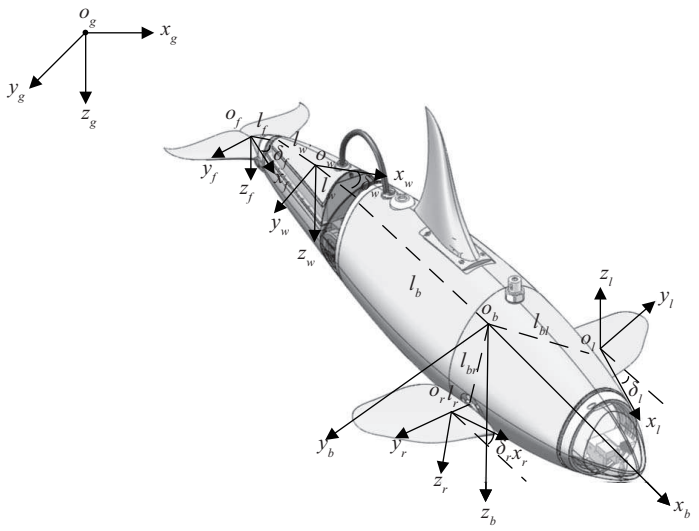

Figure 4 Schematic illustration of the reference frames.

and ζ denotes the phase lag.

3 Modeling of the robotic dolphin

3.1 Coordinate frames

We review the 3-D dynamics model of the robotic dolphin, which serves as the basis for the simulation design to verify the control strategies. To clearly describe the kinematic and dynamic modeling of the robot, the relevant coordinate frames are defined and illustrated in Figure 4.

The inertial frame is defined as {I} ($O_g x_g y_g z_g$). x_g and y_g axes lie in the horizontal plane, and z_g axis is along gravity direction. The body reference frame is labeled as {B} ($O_b x_b y_b z_b$) with its origin at the robot's center of buoyancy. The x_b and y_b axes are along the body's longitudinal axis and transverse axis, respectively. Furthermore, the control surface moving reference frames {i} ($O_i x_i y_i z_i$) are depicted, where $i = w, f, l, r$ represents the waist, fluke, left flipper, and right flipper, respectively. Each moving frame has its origin in the "middle point" of each control surface. The above coordinate frames all obey the right-hand orthonormal principle.

3.2 Kinematics

In order to facilitate robotic dolphin modeling, some reasonable assumptions are made.

(1) The fluid is assumed to be incompressible as well as irrotational, so 3-D fluid effects in the robot are neglected.

(2) During practical operations, thanks to the restoring forces of the robot, the pitch angle is not likely to be $\pm\frac{\pi}{2}$.

The following vectors are used to describe the general motion of the robotic dolphin [24]:

$$\boldsymbol{\eta} = [\boldsymbol{\eta}_1, \boldsymbol{\eta}_2]^{\mathrm{T}}, \tag{3}$$

$$\boldsymbol{\upsilon} = [\boldsymbol{\nu}_b, \boldsymbol{\omega}_b]^{\mathrm{T}}, \tag{4}$$

where $\boldsymbol{\eta}_1 = [x, y, z]^{\mathrm{T}}$ and $\boldsymbol{\eta}_2 = [\phi, \theta, \psi]^{\mathrm{T}}$ denote the inertial positions and Euler angles with coordinates in the {I} frame. $\boldsymbol{\nu}_b = [u, v, w]^{\mathrm{T}}$ and $\boldsymbol{\omega}_b = [p, q, r]^{\mathrm{T}}$ are the generalized translational and rotational velocity vectors with coordinates in the {B} frame.

The kinematic of the robot is given by

$$\dot{\boldsymbol{\eta}} = \begin{bmatrix} {}^{g}R_b & 0 \\ 0 & {}^{g}\xi_b \end{bmatrix} \boldsymbol{\upsilon}, \tag{5}$$

where ${}^{g}R_b$ is a transformation matrix in the orientation of {B} frame with respect to (w.r.t.) the {I} frame:

$${}^{g}R_b = \begin{bmatrix} \mathrm{c}\psi\mathrm{c}\theta & \mathrm{c}\psi\mathrm{s}\theta\mathrm{s}\phi - \mathrm{s}\psi\mathrm{c}\phi & \mathrm{s}\psi\mathrm{s}\phi + \mathrm{c}\psi\mathrm{c}\phi\mathrm{s}\theta \\ \mathrm{s}\psi\mathrm{c}\theta & \mathrm{c}\psi\mathrm{c}\phi + \mathrm{s}\psi\mathrm{s}\theta\mathrm{s}\phi & -\mathrm{c}\psi\mathrm{s}\phi + \mathrm{s}\theta\mathrm{s}\psi\mathrm{c}\phi \\ -\mathrm{s}\theta & \mathrm{c}\theta\mathrm{s}\phi & \mathrm{c}\theta\mathrm{c}\phi \end{bmatrix}, \tag{6}$$

and the transformation matrix ${}^{g}\xi_b$ is given by

$${}^{g}\xi_b = \begin{bmatrix} 1 & \mathrm{t}\theta\mathrm{s}\phi & \mathrm{t}\theta\mathrm{c}\phi \\ 0 & \mathrm{c}\phi & -\mathrm{s}\phi \\ 0 & \mathrm{s}\phi/\mathrm{c}\theta & \mathrm{c}\phi/\mathrm{c}\theta \end{bmatrix}, \tag{7}$$

where $\mathrm{s}(\cdot) \triangleq \sin(\cdot)$, $\mathrm{c}(\cdot) \triangleq \cos(\cdot)$, and $\mathrm{t}(\cdot) \triangleq \tan(\cdot)$. Note that ${}^{g}\xi_b$ is singular at $\theta = \pm\frac{\pi}{2}$.

The robotic dolphin can be viewed as a multilink system. Each control surface has its own body-fixed moving reference frames, and it can rotate about its y-axis (pointing out of the body). The rotation angle in counter-clockwise sense about its y-axis is denoted by δ_i $(i = w, f, l, r)$. When $\delta_i = 0$, the x-axis of the {i} frame is assumed to be coincident with x_b. The transformation matrix is defined as

$${}^{i}R_b = \begin{pmatrix} \mathrm{c}\delta_i & 0 & \mathrm{s}\delta_i \\ 0 & 1 & 0 \\ -\mathrm{s}\delta_i & 0 & \mathrm{c}\delta_i \end{pmatrix}. \tag{8}$$

As shown in Figure 4, rotational angles θ_i is obtained by

$$\theta_i = \begin{cases} \theta + \delta_i, & i = w, l, r, \\ \theta + \delta_w + \delta_f, & i = f. \end{cases} \tag{9}$$

The position of each control surface in {I} frame can be expressed as

$$\boldsymbol{\eta}_w = \boldsymbol{\eta}_1 + {}^{g}R_b l_b + {}^{g}R_w l_w, \tag{10}$$

$$\boldsymbol{\eta}_f = \boldsymbol{\eta}_1 + {}^{g}R_b l_b + {}^{g}R_w(l_w + l_{w'}) + {}^{g}R_f l_f, \tag{11}$$

$$\boldsymbol{\eta}_l = \boldsymbol{\eta}_1 + {}^{g}R_b l_{bl} + {}^{g}R_l l_l, \tag{12}$$

$$\boldsymbol{\eta}_r = \boldsymbol{\eta}_1 + {}^{g}R_b l_{br} + {}^{g}R_r l_r. \tag{13}$$

Then, the velocities of each control surface concerning the {I} frame can be derived, i.e., ${}^{g}\boldsymbol{\nu}_i = \dot{\boldsymbol{\eta}}_i$ $(i = w, f, l, r)$. Similarly, the angular velocity of each control surface concerning the {I} frame is ${}^{g}\boldsymbol{\omega}_i = {}^{g}\boldsymbol{\omega}_b + {}^{g}R_i\boldsymbol{\omega}_i$.

3.3 Kinetics

The dynamics of the robotic dolphin in 3-D space is derived from the general underwater vehicle model [24]:

$$\boldsymbol{M}\dot{\boldsymbol{\upsilon}} + \boldsymbol{C}(\boldsymbol{\upsilon})\boldsymbol{\upsilon} + \boldsymbol{D}(\boldsymbol{\upsilon})\boldsymbol{\upsilon} + \boldsymbol{g}(\boldsymbol{\eta}) = \boldsymbol{\tau}, \tag{14}$$

where $\boldsymbol{M}$ denotes the rigid-body inertial matrix and added mass owing to the inertia of the surrounding fluid. $\boldsymbol{C}(\boldsymbol{\upsilon})$ represents the Coriolis and Centripetal matrix because of the rotation of {B} frame about the {I} frame. $\boldsymbol{D}(\boldsymbol{\upsilon})$ is the hydrodynamic damping matrix in which only the linear damping is utilized for simplicity. $\boldsymbol{g}(\boldsymbol{\eta}) = \boldsymbol{W} + \boldsymbol{B}$ denotes the restoring forces and moments that are expressed in {B} frame, owing to the gravity ($\boldsymbol{W}$) and buoyancy ($\boldsymbol{B}$).

The vector $\boldsymbol{\tau}$ is the total forces and moments depending on dorsoventral oscillations of the waist and fluke, accompanied by pitch and yaw maneuvers. The hydrodynamic force acting on the fluid is usually expressed employing the wind frame {w}; that is, the force (${}^{w}\boldsymbol{F}_i$) and moment (${}^{w}\boldsymbol{\tau}_i$) acting on the control surface containing the drag, sideforce, and lift expressed in the {w} frame are

$${}^{w}\boldsymbol{F}_i = \begin{pmatrix} -\boldsymbol{D}_i \\ \mathbf{SF}_i \\ -\boldsymbol{L}_i \end{pmatrix} = \frac{1}{2}\rho\left({}^{i}\boldsymbol{v}_i\right)^2 S_i \begin{pmatrix} -C_{Di}\left(\alpha_i, \beta_i\right) \\ C_{SFi}\left(\alpha_i, \beta_i\right) \\ -C_{Li}\left(\alpha_i, \beta_i\right) \end{pmatrix}, \tag{15}$$

$${}^{\omega}\boldsymbol{\tau}_i = \begin{pmatrix} {}^{w}\boldsymbol{\tau}_x \\ {}^{w}\boldsymbol{\tau}_y \\ {}^{w}\boldsymbol{\tau}_z \end{pmatrix} = \frac{1}{2}\rho\left({}^{i}\boldsymbol{v}_i\right)^2 S_i \begin{pmatrix} C_{Mx}\left(\alpha_i, \beta_i\right) \\ C_{My}\left(\alpha_i, \beta_i\right) \\ C_{Mz}\left(\alpha_i, \beta_i\right) \end{pmatrix} + K_{\omega}{}^{i}\boldsymbol{\omega}_i, \tag{16}$$

where S_i is the area of each control surface. C_{Di}, C_{SFi}, C_{Li}, C_{Mx}, C_{My}, and C_{Mz} indicate the corresponding hydrodynamic coefficients, which are related to the angle of attack ($\alpha_i = \arctan({}^{i}\upsilon_{iz}/{}_{i}\upsilon_{ix})$) and the sideslip angle ($\beta_i = \arcsin({}^{i}\upsilon_{iy}/\|{}^{i}\upsilon_i\|)$). K_ω is the rotational damping matrix. The transformation matrix can be obtained as

$${}^{i}R_w = \begin{bmatrix} \mathrm{c}_{\alpha_i}\mathrm{c}_{\beta_i} & -\mathrm{c}_{\alpha_i}\mathrm{s}_{\beta_i} & -\mathrm{s}_{\alpha_i} \\ \mathrm{s}_{\beta_i} & \mathrm{c}_{\beta_i} & 0 \\ \mathrm{s}_{\alpha_i}\mathrm{c}_{\beta_i} & -\mathrm{s}_{\alpha_i}\mathrm{s}_{\beta_i} & \mathrm{c}_{\alpha_i} \end{bmatrix}. \tag{17}$$

In the {i} frame, the hydrodynamic forces and moments can be expressed as

$$\begin{pmatrix} \boldsymbol{F}_i \\ \boldsymbol{\tau}_i \end{pmatrix} = {}^{i}R_w \begin{pmatrix} {}^{w}\boldsymbol{F}_i \\ {}^{w}\boldsymbol{\tau}_i \end{pmatrix}, \quad i = w, f, r, l. \tag{18}$$

Finally, $\boldsymbol{\tau}$ can be obtained in the {B} frame:

$$\boldsymbol{\tau} = \begin{pmatrix} {}^{b}\boldsymbol{F}_{\text{total}} \\ {}^{b}\boldsymbol{\tau}_{\text{total}} \end{pmatrix} = \begin{pmatrix} F_b \\ \tau_b \end{pmatrix} + \begin{pmatrix} {}^{i}R_b & -{}^{i}R_b\hat{P}_i \\ 0 & {}^{i}R_b \end{pmatrix}^{\mathrm{T}} \begin{pmatrix} \boldsymbol{F}_i \\ \boldsymbol{\tau}_i \end{pmatrix}, \quad i = w, f, r, l. \tag{19}$$

4 LOS guidance principle for 3-D path following

Figure 5 depicts the block diagram of the 3-D path following control. The desired path point (x_p, y_p, z_p) is the input value for the control structure. The desired heading and pitch angles are acquired based on 3-D LOS guidance law. Then the decoupling controller assigns the desired angles to each joint of the robotic dolphin.

The geometry of the 3-D LOS guidance law is illustrated in Figure 6. Consider a geometric path continuously parametrized $P_p(\varpi) = [x_p(\varpi), y_p(\varpi), z_p(\varpi)] \in \mathbb{R}^3$, which is parameterized by a scalar

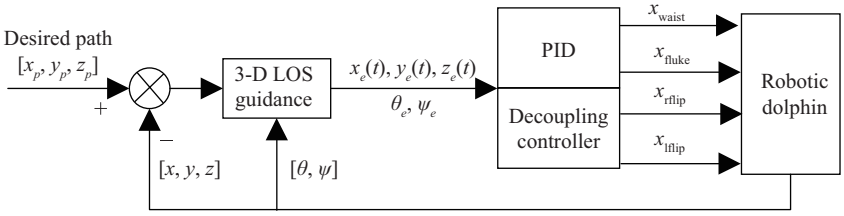

Figure 5 Control block diagram for 3-D path following system.

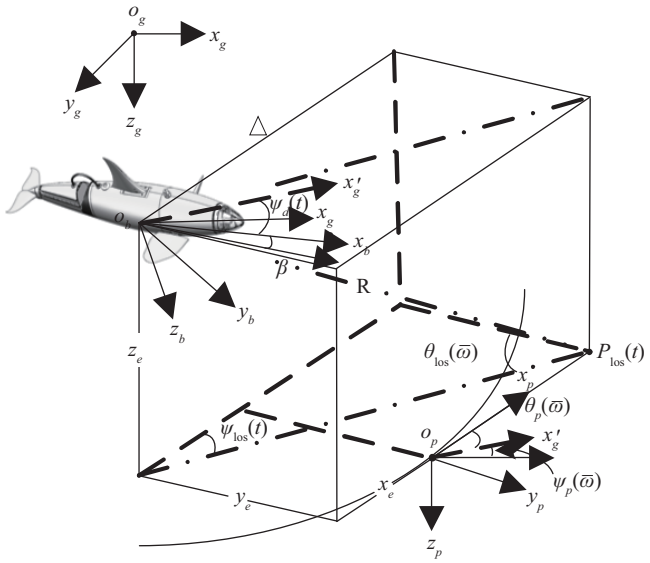

Figure 6 LOS guidance geometry for 3-D curve.

variable $\varpi \in \mathbb{R}$. As shown in Figure 6, the spatial path-fixed reference coordinate system {P} ($O_p x_p y_p z_p$) with its origin at the point $P_p(\varpi)$ is defined by a given ϖ. The $O_p x_p$-axis and $O_p y_p$-axis are along the tangent and normal of the desired path, respectively. The azimuth and elevation angles from the {I} frame to the {P} frame are defined as

$$\psi_p(\varpi) = \text{atan2}\left(\frac{\mathrm{d}y_p(\varpi)}{\mathrm{d}\varpi}, \frac{\mathrm{d}x_p(\varpi)}{\mathrm{d}\varpi}\right), \tag{20}$$

$$\theta_p(\varpi) = \text{atan2}\left(-\frac{\mathrm{d}z_p(\varpi)}{\mathrm{d}\varpi}, \sqrt{\frac{\mathrm{d}x_p(\varpi)}{\mathrm{d}\varpi}^2 + \frac{\mathrm{d}y_p(\varpi)}{\mathrm{d}\varpi}^2}\right), \tag{21}$$

where $\text{atan2}(b, a)$ is the four-quadrant version of $\arctan(b/a)$. The full rotation matrix from {P} to the {I} can be inferred as

$$^g R_p = R_{p,z}(\psi_p(\varpi)) R_{p,y}(\theta_p(\varpi)). \tag{22}$$

Subsequently, the following error vector $\varepsilon(t) \in \mathbb{R}^3$ can be defined in the {P} frame as

$$\varepsilon(t) = [x_e(t), y_e(t), z_e(t)]^{\mathrm{T}} = {}^g R_p^{\mathrm{T}}(P_p(t) - P_p(\varpi)), \tag{23}$$

where $x_e(t)$, $y_e(t)$, and $z_e(t)$ represent the along-track, cross-track, and vertical-track errors relative to $P_p(\varpi)$, respectively, which are demonstrated in Figure 6. The path following errors vector can be expanded as

$$\begin{aligned}
x_e(t) &= \mathrm{c}\psi_p(\varpi)\mathrm{c}\theta_p(\varpi)(x_p(t) - x_p(\varpi)) + \mathrm{s}\psi_p(\varpi)\mathrm{c}\theta_p(\varpi)(y_p(t) - y_p(\varpi)) - \mathrm{s}\theta_p(\varpi)(z_p(t) - z_p(\varpi)),\\
y_e(t) &= -\mathrm{s}\psi_p(\varpi)(x_p(t) - x_p(\varpi)) + \mathrm{c}\psi_p(\varpi)(y_p(t) - y_p(\varpi)),\\
z_e(t) &= \mathrm{c}\psi_p(\varpi)\mathrm{s}\theta_p(\varpi)(x_p(t) - x_p(\varpi)) + \mathrm{s}\psi_p(\varpi)\mathrm{s}\theta_p(\varpi)(y_p(t) - y_p(\varpi)) + \mathrm{c}\theta_p(\varpi)(z_p(t) - z_p(\varpi)).
\end{aligned} \tag{24}$$

Table 1 Control parameters of the robotic dolphin

Parameter	Value	Unit	Parameter	Value	Unit
m_b	6.42	kg	l_f	$(0.18, 0, 0)^{\mathrm{T}}$	m
m_w	0.87	kg	l_{bl}	$(-0.13,\ 0,\ 0.03)^{\mathrm{T}}$	m
m_f	0.10	kg	l_{br}	$(-0.13,\ 0,\ 0.03)^{\mathrm{T}}$	m
m_l	0.05	kg	S_b	0.015	m^2
m_r	0.05	kg	S_w	0.076	m^2
ρ	998	$\mathrm{kg/m}^3$	S_f	0.088	m^2
R	0.3	m	S_l	0.061	m^2
l_b	$(-0.31,\ 0,0)^{\mathrm{T}}$	m	S_r	0.061	m^2
$l_{w'}$	$(0.08,\ 0,\ 0)^{\mathrm{T}}$	m	l_w	$(0.09,\ 0,\ 0)^{\mathrm{T}}$	m
l_l	$(0,\ 0.06,\ 0)^{\mathrm{T}}$	m	l_r	$(0,\ 0.06,\ 0)^{\mathrm{T}}$	m

The associated control objective for the 3-D spatial path following becomes

$$\lim_{t\to\infty} y_e(t) = 0, \quad \lim_{t\to\infty} z_e(t) = 0. \tag{25}$$

The traditional guidance based path following scheme used by [20, 25–27] would set the vessel heading and pitch angles to shape the convergence behavior toward the xz-plane and xy-plane of the path-fixed frame. However, in this paper, the different guidance law based on the lookahead steering is proposed to reduce the overall complexity.

Consider a sphere with radius R enclosing the robotic dolphin's center of buoyancy. If the radius is chosen to be sufficiently large, it will intersect the path tangentially at the foresight point $P_{\mathrm{los}}(t)$. The lookahead based guidance law is given by

$$\begin{aligned} &\psi_{\mathrm{los}}(t) \doteq \mathrm{atan2}(y_e(t), \Delta), \\ &\theta_{\mathrm{los}}(t) \doteq \mathrm{atan2}\left(z_e(t), \sqrt{y_e(t)^2 + \Delta^2}\right), \end{aligned} \tag{26}$$

where Δ is a time-varying guidance variable that is positive and upper bounded. Furthermore, Δ can be calculated by

$$\Delta^2 + {y_e}^2 + {z_e}^2 = R^2. \tag{27}$$

Finally, the desired heading and pitch angles can be obtained according to Figure 6:

$$\psi_d(t) = \psi_p(\varpi) - \psi_{\mathrm{los}}(t) - \beta, \quad \theta_d(t) = \theta_p(\varpi) - \theta_{\mathrm{los}}(t) + \alpha, \tag{28}$$

where α and β are angles of attack and sideslip, respectively.

5 Simulation and analysis

For the sake of testing the feasibility of the decoupling strategy and the LOS based path following controller, numerical simulations are carried out in the robotic dolphin, whose parameters are listed in Table 1. The simulations ran on a desktop computer with Intel(R) Core(TM) i7-8550U 1.99 GHz CPU and 16 GB of RAM, running win10 and coding in MATLAB 2019.

5.1 Decoupling motion

The depth control is assumed to conduct in xz-vertical plane, and the desired depth is parameterized as

$$\begin{aligned} &z_p(t) = -1, \qquad x_p \leqslant 50, \\ &z_p(t) = -2, \qquad 50 < x_p \leqslant 120. \end{aligned} \tag{29}$$

In the vertical plane, $\psi_p(t) = 0$, $\theta_p(t) = 0$, and $\theta_d(t) = -\theta_{\mathrm{los}}(t) + \alpha$. Comparison of depth plotted against x_p for the robotic dolphin is illustrated in Figure 7, followed by a time history of the pitch angle. The pitch angle has an excellence response to the desired pitch angle. It indicates that decoupled pitch maneuver and LOS guidance law can steer the robot toward and along with the desired depth.

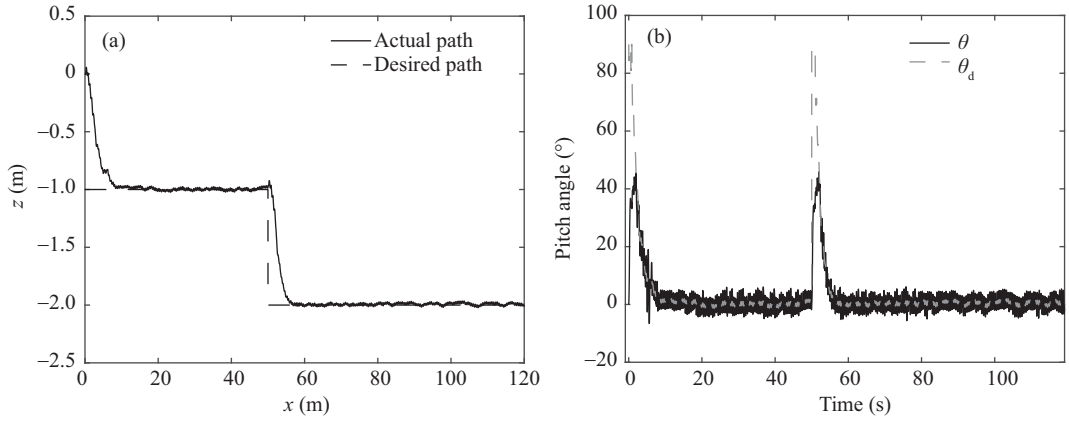

Figure 7 Depth control. (a) Depth control response; (b) time history of pitch angle.

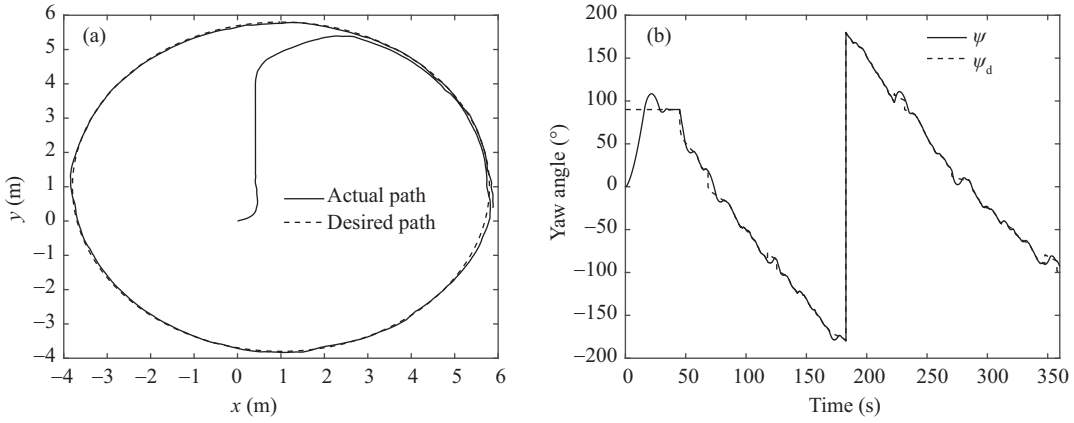

Figure 8 Planar path following. (a) Path following response; (b) time history of yaw angle.

Next, the planar path following control is conducted, and the predefined planar path is defined as

$$\begin{aligned} x_p(\varpi) &= 4.8\sin(\varpi) + 1, \qquad 0 \leqslant \varpi \leqslant 2\pi, \\ y_p(\varpi) &= 4.8\cos(\varpi) + 1, \qquad 0 \leqslant \varpi \leqslant 2\pi. \end{aligned} \tag{30}$$

The simulation results are demonstrated in Figure 8. It is clear that the robotic dolphin moves toward and along the desired path, and the yaw angle has an excellent response to the reference angle (the average heading-track error is 1.37°), which verifies the effectiveness of the proposed strategies.

5.2 3-D path following

Finally, the 3-D path following simulation concerning a spatial helix is carried out in the robotic dolphin, which is parameterized by ϖ as

$$\begin{aligned} x_p(\varpi) &= 50\sin(\varpi), & -10 \leqslant \varpi \leqslant 10, \\ y_p(\varpi) &= 50\cos(\varpi) - 50, & -10 \leqslant \varpi \leqslant 10, \\ z_p(\varpi) &= -0.5\varpi, & -10 \leqslant \varpi \leqslant 10. \end{aligned} \tag{31}$$

The initial positions and attitude angles of the robotic dolphin are all set as zero. To solve the intersection point between the 3-D helix and sphere, the "polyxpoly" function in MATLAB is utilized. The 3-D path following response of the robotic dolphin is illustrated in Figure 9, where it is easily seen that the robot nicely converges toward and moves along the desired helix path. Furthermore, Figure 10 shows that the cross-track and vertical-track errors converge to and oscillate at the reasonable level (the averages are 0.04 m and 0.012 m, respectively). The essence of the path following control is to track the desired yaw and pitch angles. Based on (28), the desired yaw and pitch angles are calculated and depicted in Figure 11. It is clear that the robot has a steady-state oscillatory behavior when it reaches the desired

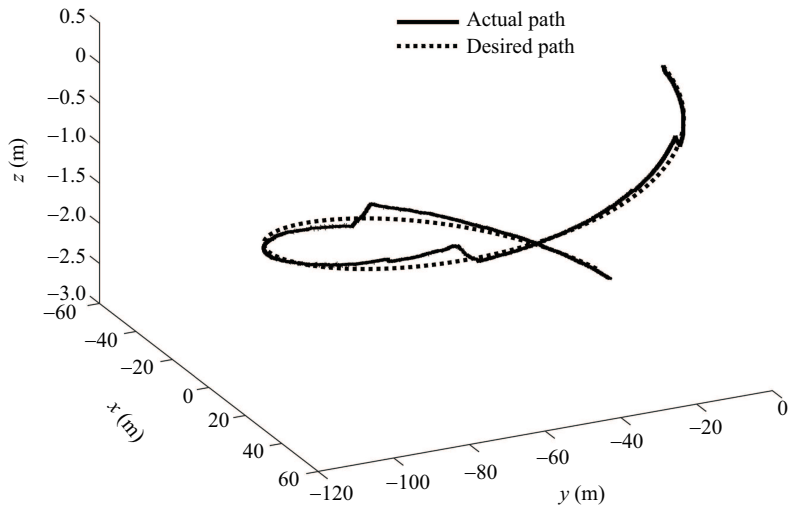

Figure 9 LOS guidance geometry for 3-D curve.

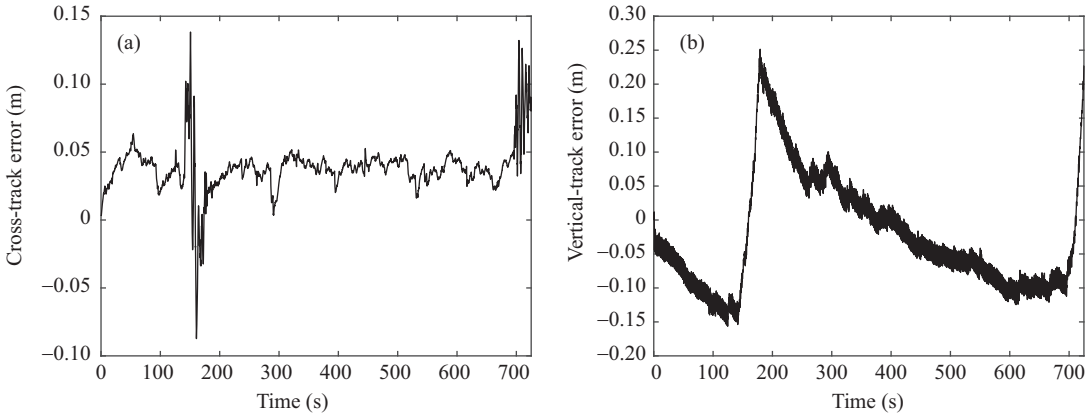

Figure 10 Path following errors. (a) Cross-track error; (b) vertical-track error.

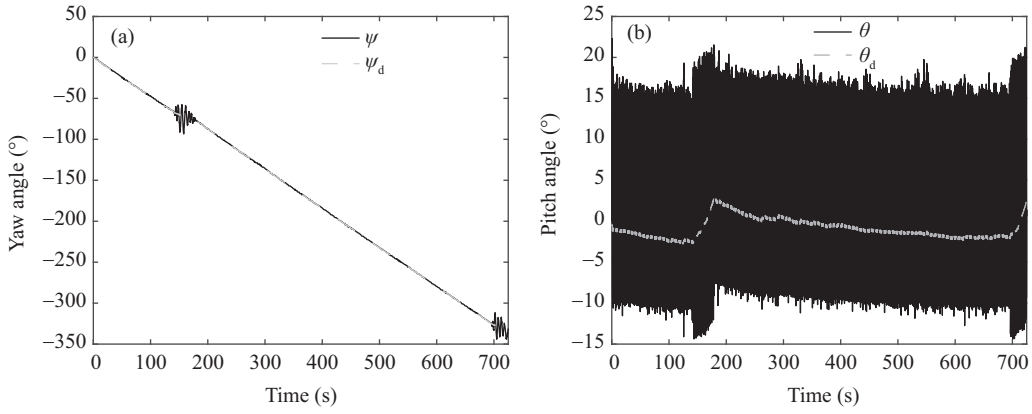

Figure 11 Time history of attitude during the path following. (a) Yaw angle; (b) pitch angle.

path. Note that it would still oscillate owing to the oscillating motion of the waist joint and fluke. The pitch angle gradually stable during the following control has small oscillations with an amplitude about 15°. The success of 3-D path following testifies the effectiveness and feasibility of the designed decoupling strategy and LOS guidance law.

5.3 Discussion

With consideration of dolphin-like swimming, symmetrical and dorsoventral oscillations can be regarded as an active way of producing thrust forces, while asymmetrical oscillations of waist and fluke in conjunction with asymmetrical flapping of flippers yield different maneuvers. Based on this performance, the decoupling motion can be achieved. Compared with the multilink dolphin-like robot [7], whose mechanical structure consists of a yaw joint and three pitch joints, the utilized robotic dolphin has a more straightforward structure and achieves better yaw maneuver than pitch maneuver. Compared with [21], lookahead based 3-D LOS guidance law reduces the computational complexity by calculating the intersection between sphere and curve. The guidance law has a better prospect of application.

However, as depicted in Figure 7, the mean pitch angle error is about $\pm 3.5^\circ$, which is larger then [10] whose average is $\pm 1.466^\circ$. It means the flippers are more suitable for handling depth control. In the context of 3-D path following, the proposed decoupling strategy has application potential with the sacrifice of control accuracy. Further study involves soft robots that provide a better 3-D maneuver solution.

6 Conclusion

In this paper, we have offered a 3-D path following solution for a robotic dolphin, which provides a tradeoff between the 3-D maneuverability and the structural complexity. More specifically, a comprehensive 3-D dolphin-like swimming model is carried out. Next, control strategies consisting of decoupling control and 3-D LOS based guidance law are proposed to achieve path following. Finally, simulations on the robotic dolphin testify the effectiveness. This study sheds light on intelligent control of robotic dolphins in 3-D environments, contributing to updated design and control of innovative fish or dolphin inspired swimming robots.

For future work, the decoupling strategy and LOS guidance law will be systematically implemented and improved on the actual robotic dolphin platform. In addition, combining sliding mode control or reinforcement learning with 3-D path following method will be explored to advance the applications of robotic dolphin in real ocean-oriented scenarios.

Acknowledgements This work was supported by National Natural Science Foundation of China (Grant Nos. 61903007, 61633017, 61633004, 61725305, 61973007, U1909206), Pre-research Fund of Equipment of China (Grant No. 61402070304), Key Research and Development and Transformation Project of Qinghai Province (Grant No. 2017-GX-103), and Youth Innovation Science and Technology Plan of Shandong Province (Grant No. 2019KJN015).

References

1 Yu J Z, Wu Z X, Su Z S, et al. Motion control strategies for a repetitive leaping robotic dolphin. IEEE/ASME Trans Mechatron, 2019, 24: 913–923
2 Yao P, Qi S B. Obstacle-avoiding path planning for multiple autonomous underwater vehicles with simultaneous arrival. Sci China Technol Sci, 2019, 62: 121–132
3 Nakashima M, Tsubaki T, Ono K. Three-dimensional movement in water of the dolphin robot-control between two positions by roll and pitch combination. J Robot Mechatron, 2006, 18: 347–355
4 Wu Z X, Yu J Z, Yuan J, et al. Gliding motion regulation of a robotic dolphin based on a controllable fluke. IEEE Trans Ind Electron, 2020, 67: 2945–2953
5 Wu Z X, Yu J Z, Yuan J, et al. Towards a gliding robotic dolphin: design, modeling, and experiments. IEEE/ASME Trans Mechatron, 2019, 24: 260–270
6 Wang J, Wu Z X, Tan M, et al. 3-D path planning with multiple motions for a gliding robotic dolphin. IEEE Trans Syst Man Cybern Syst, 2019. doi: 10.1109/TSMC.2019.2917635
7 Yu J Z, Su Z S, Wang M, et al. Control of yaw and pitch maneuvers of a multilink dolphin robot. IEEE Trans Robot, 2012, 28: 318–329
8 Shen F, Wei C M, Cao Z Q, et al. Implementation of a multi-link robotic dolphin with two 3-DOF flippers. J Comput Inform Syst, 2010, 7: 2601–2607
9 Wang Y L, Tai C H, Huang H R. Design and development of an autonomous underwater vehicle-robot dolphin. J Mar Eng Tech, 2015, 14: 44–55
10 Yu J Z, Liu J C, Wu Z X, et al. Depth control of a bioinspired robotic dolphin based on sliding-mode fuzzy control method. IEEE Trans Ind Electron, 2018, 65: 2429–2438
11 Liu J C, Wu Z X, Yu J Z, et al. Sliding mode fuzzy control-based path-following control for a dolphin robot. Sci China Inf Sci, 2018, 61: 024201
12 Park S S. Design of three-dimensional path following guidance logic. Int J Aerosp Eng, 2018, 2018: 9235124
13 Zheng Z W, Sun L, Xie L H. Error-constrained LOS path following of a surface vessel with actuator saturation and faults. IEEE Trans Syst Man Cybern Syst, 2018, 48: 1794–1805
14 Breivik M, Fossen T I. Path following for marine surface vessels. In: Proceedings of IEEE Techno-Ocean'04, 2004. 2282–2289
15 Wang Y H, Tong H Y, Fu M Y. Line-of-sight guidance law for path following of amphibious hovercrafts with big and time-varying sideslip compensation. Ocean Eng, 2019, 172: 531–540
16 Bai T T, Wang D B. Cooperative trajectory optimization for unmanned aerial vehicles in a combat environment. Sci China Inf Sci, 2019, 62: 010205

17 Kelasidi E, Liljeback P, Pettersen K Y, et al. Integral line-of-sight guidance for path following control of underwater snake robots: theory and experiments. IEEE Trans Robot, 2017, 33: 610–628
18 Caharija W, Pettersen K Y, Bibuli M, et al. Integral line-of-sight guidance and control of underactuated marine vehicles: theory, simulations, and experiments. IEEE Trans Contr Syst Technol, 2016, 24: 1623–1642
19 Lekkas A. Guidance and path-planning systems for autonomous vehicles. Dissertation for Ph.D. Degree. Trondheim: Norwegian University of Science and Technology, 2014
20 Zuo Z Y, Cheng L, Wang X X, et al. Three-dimensional path-following backstepping control for an underactuated stratospheric airship. IEEE Trans Aerosp Electron Syst, 2019, 55: 1483–1497
21 Breivik M, Fossen T I. Principles of guidance-based path following in 2D and 3D. In: Proceedings of IEEE International Conference on Decision Control, Seville, 2005. 627–634
22 Wang G X, Xu G H, Liu G, et al. Fuzzy iterative sliding mode control applied for path following of an autonomous underwater vehicle with large inertia. Math Probl Eng, 2019, 2019: 8650243
23 Liu J C, Wu Z X, Yu J Z, et al. Flippers-based turning analysis and implementation of a dolphin robot. In: Proceedings of IEEE International Conference on Robotics and Biomimetics, Macao, 2017. 141–146
24 Fossen T I. Handbook of Marine Craft Hydrodynamics and Motion Control. United Kingdom: John Wiley & Sons Ltd, 2011
25 Xiang X B, Yu C Y, Zhang Q. Robust fuzzy 3D path following for autonomous underwater vehicle subject to uncertainties. Comput Oper Res, 2017, 74: 165–177
26 Yu C Y, Xiang X B, Dai J R. 3D path following for underactuated AUV via nonlinear fuzzy controller. In: Proceedings of OCEANS 2016, Shanghai, 2016. 1–7
27 Breivik M, Fossen T I. Guidance Laws for Autonomous Underwater Vehicles. Rijeka: InTech, 2009